EPJ manuscript No.
(will be inserted by the editor)

Stick slip displacement of confined granular mixtures: bubble expansion

Bjørnar Sandnes[1,2,a], Eirik Grude Flekkøy[3] and Knut Jørgen Måløy[3]

[1] Department of Physics, Norwegian University of Science and Technology, Hoegskoleringen 5, N-7491 Trondheim, Norway
[2] School of Chemical and Biomolecular Engineering, University of Sydney, Sydney, New South Wales 2006, Australia
[3] Department of Physics, University of Oslo, Sem Sælands vei 24, PO Box 1048 Blindern, 0316 Oslo, Norway

Abstract. When a compressible gas displaces a granular mixture in a quasi 2D space, friction causes stick slip motion. A localized slip event at the interface allows expansion of the compressed gas and a sudden forward motion of the front. The reservoir volume of gas determines the available elasticity in the system, and thereby the size of the expansion. Large expansions take the shape of bubbles, and in this paper we study the accumulation of granular material around the inflating gas bubble, and the rheological response of the system during this short expansion phase.

1 Introduction

The displacement of one fluid by another occurs in a range of natural and industrial settings. One example is oil recovery, where saline water replaces viscous oils extracted from the inter-particle space in porous reservoirs. Another application gaining considerable attention is the injection of CO_2 into suitable underground geological formations for mitigation of greenhouse gas emissions.

Complex interplays between acting forces during these displacement processes give rise to hydrodynamic instabilities and pattern formation. Viscous fingering involving both Newtonian and non-Newtonian fluids [1–4], and two-phase flow in porous media are well known examples [1, 5–7]. Recently, the flow behaviour and pattern formation of granular fluid mixtures have come to the forefront of current research [8–15], motivated both by the rich diversity of physical phenomena observed, and the pervasiveness of these materials in engineered processes and the environment.

In a recent paper we considered the displacement of confined granular mixtures [16], and found crossovers between a range of pattern forming states depending on the experimental parameters (injection rate, filling fraction and compressibility). The dynamic states include viscous fingering at high rates, fracturing at high filling fractions, and frictional fingering and stick slip bubbles at low rate and low to intermediate filling fractions.

[a] e-mail: bjornar.sandnes@ntnu.no

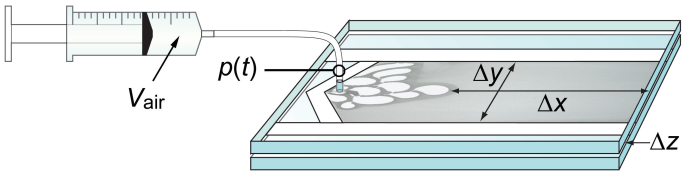

Fig. 1. Sketch of the experimental cell. Air is slowly injected into the gap of the cell containing the granular fluid mixture.

In this paper we focus on the frictional regime at low rate, and specifically the mode in which large bubbles of air displace the granular mixture. While the static friction of the jammed front determines the yield pressure of the bubble, the expansion of the bubble is governed by the local accumulation of granular material, and the rheological response of the overall system. We show that a simple mathematical model incorporating the rheology of the local granular front and the flow channel, as well as capillary and frictional forces reproduces the pressure evolution during bubble expansion well.

2 Experiments

A mixture of a granular material - 100 μm diameter polydisperse glass beads - and a 50 % water/glycerol solution is loaded into the gap between two parallel glass plates of a Hele-Shaw channel. The plates are bonded together with double sided tape forming a 20x30 cm channel with a gap height of Δz = 0.5 mm (Fig. 1). A 5 mm diameter inlet hole is positioned at one end of the channel, and the opposite end of the channel is open to the surrounding air. After loading, the granular material settles out of suspension onto the lower glass plate. The height of the granular layer relative to the gap height corresponds to the filling fraction φ of granular material in the mixture which is normalized such that $\varphi = 1$ for closely packed grains. $\varphi = 0.58$ for the experiments presented here.

The experiment commences by slowly injecting air into the cell using a syringe pump (WPI, Alladin) set to a constant volume flow rate q, typically 0.01-0.03 ml/min. The volume of air, V_{air}, initially contained in the syringe determines the total compressibility of the system, or, alternatively, the volumetric stiffness defined as $K = P_0/V_{air}$, where P_0 is the pressure of the surroundings [16].

A camera (PL-B742U, Pixelink) is placed underneath the cell and acquires images in time lapse mode. The cell is back-lit using a white screen and two high frequency fluorescent lights. A pressure sensor (HCL0075D, Sensor Technics) connected to a DAQ system (NI cDAQ 9172, NI 9237, National Instruments) measures and records the gas pressure during the experiment.

3 Stick slip dynamics

The slowly advancing air/fluid interface accumulates a front of granular material that fills the gap from top to bottom [13]. Depending on the experimental parameters, two distinct morphologies can emerge: frictional fingers (low φ, high K) or stick slip bubbles (high φ, low K) [16].

The bubbles, Fig. 2(a), appear for high yield pressures (high φ gives a thick granular front and therefore high friction), and for large compressibility as determined by

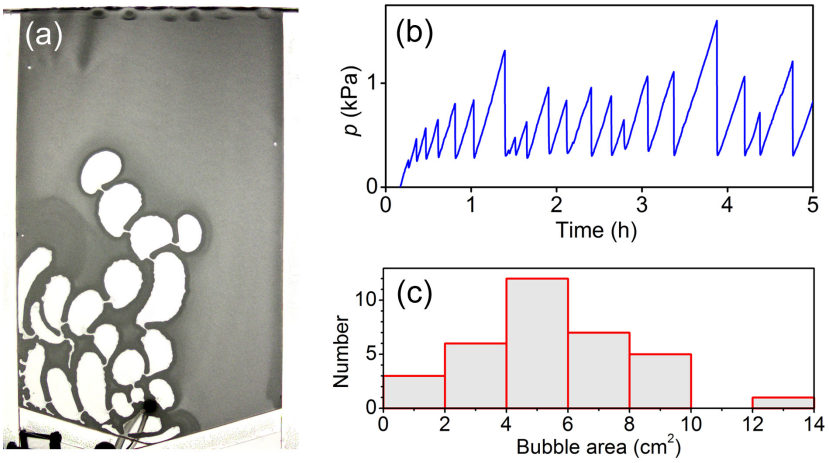

Fig. 2. (a) Gas bubbles appear one by one as a result of the slow injection of air into the confined granular mixture. The cell is 20 cm wide, placed horizontally and imaged from below. (b) Gas pressure during the displacement process. (c) Size distribution (area) of the bubbles after the completion of the experiment.

the gas reservoir volume V_{air}. Fig. 2(b) shows the gas pressure during the displacement process. A jammed granular front causes the pressure to build gradually as the pump compresses the air at a constant rate. When the gas pressure reaches the yield stress of the granular front, the packing deforms and air penetrates the front and expands radially in the shape of a bubble as the air decompresses. The pressure thus decreases rapidly, and the expansion of the bubble stops. This kind of intermittent motion is analogous to the stick slip sliding of a spring-block system on a frictional surface. The intermittency has further some analogy to Haines jumps in porous media [17–19]. However an important difference is that there is no Coulomb friction, only viscous friction connected to the Haines Jumps.

The constant pumping drives the system through compression/expansion cycles progressively filling the cell with bubbles as seen in Fig. 2(a) and indicated by the saw-tooth pressure signature in Fig. 2(b). The size of the bubbles are proportional to the pressure drop during the expansion. Fig. 2(c) shows the size distribution of the bubbles in the experiment presented in (a). The size distribution is fairly wide, with a mean bubble size of 5.7 cm^2, corresponding to a gas volume of approximately 0.3 ml.

Note that there is a more or less constant baseline pressure that the system relaxes to after each bubble expansion (Fig. 2(b)). The relaxation pressure seems to be independent of the size of the bubble, even though larger bubbles are surrounded by a thicker granular front. This indicates that friction is largely demobilized during the slip events, and, as we shall see in the following section, the baseline pressure is almost entirely a result of the capillary pressure associated with the out-of-plane curvature of the fluid meniscus in the cell.

4 Pressure during expansion

The bubble expansion phase is fast (10-20 s) compared to the pressure build-up (stick) phase (10-30 min) and duration of the experiments (typically 5-15 hours) (see Fig. 3 and Fig. 4). We assume isothermal expansion of an ideal gas, such that the

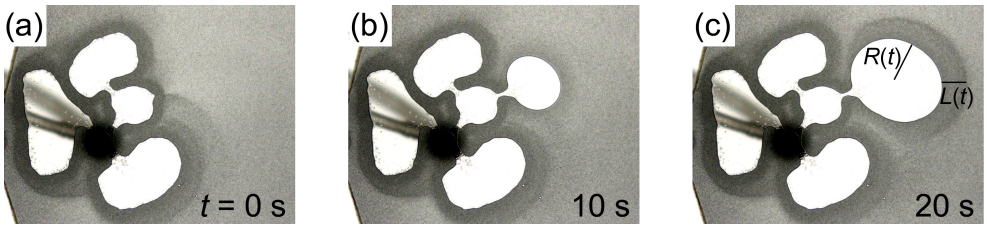

Fig. 3. (a)-(c) Time series showing the growth of a single bubble.

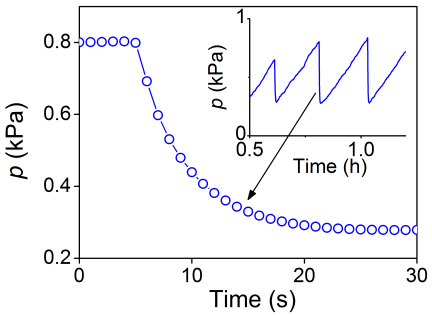

Fig. 4. The measured gas pressure during the bubble inflation depicted in Fig. 3.

pressure drop associated with the bubble inflation is $\Delta p(t) \approx -P_0 V_b(t)/V_{air}$, where $V_b(t) = \Delta z \pi R(t)^2$ is the volume of a growing bubble of radius $R(t)$. The pressure during the inflation phase becomes

$$p(t) = \sigma_{yield} - \frac{P_0}{V_{air}} \Delta z \pi R(t)^2, \tag{1}$$

or, expressed in terms of the granular friction σ, capillary pressure p_{cap}, the pressure drop due to viscous dissipation across the granular front p_g, and the viscous pressure drop associated with the flow in the Hele-Shaw cannel p_{ch}:

$$p(t) = \sigma + p_{cap} + p_g + p_{ch}. \tag{2}$$

σ has a maximal value of σ_{yield} for the jammed front, but becomes demobilized upon slip when the granular front is fluidized. The capillary (Laplace) pressure associated with the fluid/air interface is

$$p_{cap}(t) = \frac{2\gamma}{\Delta z} + \frac{\gamma}{R(t)}, \tag{3}$$

where γ is the surface tension of the fluid and we have assumed a contact angle of $\theta_C = 0^\circ$ between the fluid and the confining plates. The out-of-plane contribution to the capillary pressure is constant, and the in-plane capillary pressure is large initially but becomes insignificant as the bubble radius grows larger.

The growing bubble sweeps up and accumulates granular material into a layer of thickness $L(t)$ surrounding the air/fluid interface (Fig. 3(c)). The relation between $L(t)$ and radius $R(t)$ for a circular bubble is

$$L(t) = \Big(\frac{1}{\sqrt{1-\varphi}} - 1\Big) R(t). \tag{4}$$

In this simplified model we shall assume that this layer of granular material is dense, fluidized, and has an effective viscosity η_g. We make the assumption that p_g results from a Poiseuille flow of the granular suspension, or slurry, ahead of the advancing meniscus. This implies the assumption of an effective no-slip boundary condition along the glass plates. This is most certainly true to an excellent approximation for the pure liquid phase of viscosity η. However, since $\eta << \eta_g$ we are likely to get a high shear layer between the plates and the granular packing, which modifies the simple picture of a Poiseuille flow of the η_g phase. Still, with these reservations in mind we follow [20], from which we obtain

$$\frac{dR}{dt} = \frac{(\Delta z)^2 p_g}{12\eta_g R(t)\ln((R+L)/R)}, \tag{5}$$

and, noting that $(R+L)/R = 1/\sqrt{1-\varphi}$, we have the pressure drop over the front:

$$p_g = -\frac{6\eta_g \ln(1-\varphi)}{(\Delta z)^2} R(t)\frac{dR}{dt}. \tag{6}$$

We take as a reasonable assumption that $\varphi \approx 0.8-0.9$ in the partially compacted, fluidized granular layer surrounding the bubble. Following Stickel and Powell [21] we use $\eta_g = f(\varphi)\eta$ as an expression for the effective viscosity of the granular suspension, where $f(\varphi)$ is determined empirically, and η is the viscosity of the fluid. The empirical data presented in this paper [21] suggests a value of $f(\varphi)$ of approximately $f_g \approx 60$ for the fluidized granular front. The viscosity factor f_g depends sensitively on φ, and as a consequence, η_g has a large uncertainty associated with it.

As the bubble expands, the fluid is expelled at the far edge of the Hele-Shaw cell. For simplicity we model the fluid flow as a plane Poiseuille flow through the channel, and use an effective viscosity for the granular mixture $\eta_m = f(\varphi)\eta$ as before. Here, φ corresponds to the filling fraction of granular material in the cell overall ($\varphi = 0.58$), such that $\eta_m = f_m\eta$ with $f_m \approx 4$ estimated from the empirical data in [21]. The viscous pressure drop along the channel is

$$p_{ch} = \frac{12\eta_m \Delta x}{(\Delta z)^3 \Delta y}\frac{dV}{dt} = \frac{24\pi\eta_m \Delta x}{(\Delta z)^2 \Delta y} R(t)\frac{dR}{dt}, \tag{7}$$

where Δx is the distance between the bubble and the edge of the cell, and Δy is the channel width (see Fig. 1).

Solving equations (1-7) with respect to dR/dt yields the following differential equation:

$$\frac{dR}{dt} = a[bR(t)^{-1} - \gamma R(t)^{-2} - cR(t)], \tag{8}$$

where

$$a = \frac{\Delta y(\Delta z)^2}{6\eta}[12 f_m \pi \Delta x - 3 f_g \Delta y \ln(1-\varphi)]^{-1}, \tag{9}$$

$$b = \sigma_{yield} - \frac{2\gamma}{\Delta z}, \tag{10}$$

and

$$c = \frac{P_0}{V_{air}}\pi \Delta z. \tag{11}$$

Equation 8 is solved using a standard Matlab Ordinary Differential Equation solver (ode45). Fig. 5 shows the model prediction for gas pressure superimposed on experimental data for a single bubble which was generated approximately in the

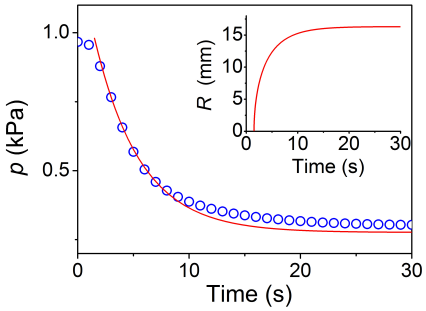

Fig. 5. Gas pressure as a function of time during bubble expansion, showing both experimental data (circles) and model output(lines). Inset: Model result for bubble radius as a function of time.

middle of the channel ($\Delta x \approx 15cm$). Here the pressure is calculated as $p(t) = \sigma_{yield} - (P_0/V_{air})\Delta z \pi R(t)^2$ using the differential equation solution for $R(t)$ (inset). The following parameter values were used: $\eta = 10$ mPa s, $f_g = 60$, $\gamma = 0.068$ N m^{-1}, $\mu = 0.4$, $\rho = 650$ kg m^{-3} (adjusted for the packing fraction of the grains), and $P_0 = 101$ kPa.

The model reproduces the dynamics reasonably well, especially for the initial stage when the front velocity is high. The model baseline pressure is determined by the constant contribution from the out-of-plane capillary pressure alone, and Fig. 5 shows that the experimentally observed baseline pressure is somewhat higher.

The rheology of the dense granular mixture is undoubtedly more complex than assumed is this simple model. The velocity of the interface is slow towards the end of the expansion phase, and it is likely that gravity induced sliding friction between the grains and the plate is mobilized, such that when the expansion slows, the gas pressure is balanced by an additional frictional stress from the layer of accumulated grains. In order to indirectly account for this effect, we introduce a (rate independent) friction between the granular packing and the plate which grows linearly with $L(t)$:

$$\sigma = \rho g \mu L(t), \tag{12}$$

where ρ is the density contrast between the granular packing and the fluid, g the gravitational acceleration, and μ the effective friction coefficient of the granular material against the glass plate. Note that this friction component is small, and only becomes significant as L becomes large towards the end of the expansion phase, coinciding with the diminishing contribution from viscous dissipation as the rate decreases. This frictional component enters the ODE as a constant term in Equation (8).

Fig. 6 shows the results of the modified model superimposed on the same experimental data as before. The small additional frictional stress increases the baseline pressure, which now is in close agreement with the experimental measurements. The figure also illustrates the dependency on the choice of viscosity factor for the dense granular front. The solid line shows the model output using a viscosity factor of $f_g = 60$, while the dotted and dashed lines show results for a viscosity factor of 40 and 80 respectively.

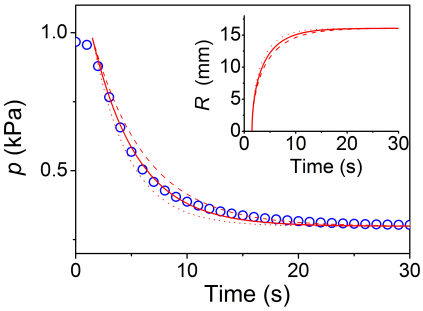

Fig. 6. Gas pressure for model with frictional component (lines). The solid line corresponds to a viscosity factor of $f_g = 60$, while the dotted and dashed lines correspond to viscosity factors of 40 and 80 respectively. Inset: Model result for bubble radius as a function of time.

5 Conclusion

We find that the model fits the experimental data well, with the pressure decreasing in an exponential fashion during the bubble inflation. The time scale of the process is set by the viscous response to the flow in the channel, with additional viscous dissipation occurring in the compacted, fluidized granular front. The constant capillary pressure of the meniscus in the gap between the plates sets the baseline pressure, with a small contribution from sliding friction between the granular material and the plate. Note that the model makes a number of simplistic assumptions, particularly regarding the flow in the channel and the way in which granular material accumulates onto the advancing bubble interface, however, the details here seem to be of secondary importance for the overall pressure evolution.

References

1. P. G. Saffman, G.Taylor, Proc. R. Soc. Lond Ser. A **245**, 1242 (1958).
2. E. Lemaire, P. Levitz, G. Daccord, H. Vandamme, Phys. Rev. Lett. **67**, 15 (1991).
3. D. Bonn, H. Kellay, M.Benamar, J. Meunier, Phys. Rev. Lett., **75**, 11 (1995).
4. A. Lindner, D. Bonn, E. C. Poire, M. Ben Amar, J.Meunier, J. Fluid Mech. **469**, (2002).
5. R. Lenormand, Physica A, **140**, 1-2 (1986).
6. K.J. Måløy, J. Feder, T. Jøssang, Phys. Rev. lett. **55**, 24 (1985).
7. Y. Meheust, G. Løvoll, K. J. Måløy, J. Schmittbuhl, Phys. Rev. E **66**, 5 (2002).
8. N. Huang, G. Ovarlez, F. Bertrand, S. Rodts, P. Coussot, D. Bonn, Phys. Rev. Lett. **94**, 2 (2005).
9. Ø. Johnsen, C. Chevalier, A. Lindner, R. Toussant, E. Clement, K. J. Måløy, E. G. Flekkøy, J. Schmittbuhl, Phys.Rev. E **78**, 5 (2008).
10. X. Cheng, L. Xu, A. Patterson, H. M. Jaeger, S. R. Nagel, Nat. Phys. **4**, 3 (2008).
11. C. Chevalier, A. Lindner, E. Clement, Phys. Rev. Lett. **99**, 17 (2007).
12. C. Chevalier, A. Lindner, M. Leroux, E. Clement, J. Non-Newton. Fluid Mech. **158**, 63 (2009).
13. B. Sandnes, H. A. Knudsen, K. J. Måløy, E. G. Flekkøy,Phys. Rev. Lett. **99**, 3 (2007).
14. H. A. Knudsen, B. Sandnes, E. G. Flekkøy, K. J. Måløy, Phys. Rev. E **77**, 2 (2008).
15. A. Fall, F. Bertrand, G. Ovarlez, D. Bonn, Phys. Rev. Lett. **103**, 17 (2009).
16. B. Sandnes, E. G. Flekkøy, H. A. Knudsen, K. J. Måløy, H. See, Nat. Commun. **2**, 288 (2011).
17. W. B. Haines, J. Agric. Sci. **20**, 97 (1930).

18. K. J. Måløy, L. Furuberg, J. Feder and T. Jøssang, Phys. Rev. Lett. **68**, 14 (1992).
19. L. Furuberg, K. J. Måløy, and J. Feder, Phys. Rev. E. **53**, 53 (1996).
20. K. T. McDonald, eprint arXiv:physics/0006067, (2000).
21. J. J. Stickel, R. L. Powell, Annu. Rev. Fluid Mech. **37**, 129 (2005).